



# Large $\mathbf{E} \times \mathbf{B}$ convection near the divertor $X$ -point

M.J. Schaffer<sup>a,\*</sup>, J.A. Boedo<sup>b</sup>, R.A. Moyer<sup>b</sup>, T.N. Carlstrom<sup>a</sup>, J.G. Watkins<sup>c</sup>

<sup>a</sup> General Atomics, P.O. Box 85608, San Diego, CA 92186-5608, USA

<sup>b</sup> University of California, San Diego, CA, USA

<sup>c</sup> Sandia National Laboratories, Albuquerque, NM, USA

## Abstract

Electric potential, electron temperature, and electron density were measured in two dimensions ( $R, Z$ ) throughout the divertor and  $X$ -point in DIII-D tokamak plasmas. An electric potential hill ( $\sim 100$  eV) and an associated electron pressure hill were discovered at the divertor  $X$ -point in L-mode plasmas. The potential hill extends previously reported divertor  $\mathbf{E} \times \mathbf{B}$  circulation, convecting particles, energy and toroidal momentum into and out of closed magnetic surfaces, and contributes significantly to transport across the boundary. The potential is explained by classical parallel (to  $\mathbf{B}$ ) plasma physics, when the  $X$ -point  $T_i$  is clamped lower than upstream  $T_i$ . The low  $X$ -point  $T_i$  state might be self-sustaining at low heating power due to the same  $\mathbf{E} \times \mathbf{B}$  circulation. We speculate that if the circulation transport is incompatible with H-mode, then the spontaneous L–H transition might require as a precondition that the  $X$ -point  $T_i$  become equalized on the near-separatrix magnetic surfaces. © 2001 Elsevier Science B.V. All rights reserved.

**Keywords:** Electric potential; Electric field;  $\mathbf{E} \times \mathbf{B}$  drift

## 1. Introduction

Many tokamaks divert exhaust plasma along magnetic lines to target surfaces somewhat removed from the main plasma. The  $X$ -point, a null point of the poloidal magnetic field in conventionally diverted tokamaks, defines a separatrix, inside of which hot plasma is confined on closed toroidal magnetic surfaces. Outside the separatrix is the scrape-off layer (SOL), where plasma flows almost parallel to the magnetic field  $\mathbf{B}$  along open magnetic lines to the target(s), where it deposits its energy and recombines. We restrict our attention to single-null divertors. See Fig. 1. In this paper, ‘the divertor’ is the region roughly between the  $X$ -point and the targets, and the ‘private region’ lies between the separatrix strike points on the target. The  $X$ -point region is complex, because four plasma regions, each with distinct

temperature, density and electric potential, meet there. Steep gradients and boundary layers are to be expected [1].

Parallel (to  $\mathbf{B}$ ) flow is clearly important in the SOL, and it has been the focus of a large body of experimental and theoretical research. Perpendicular (to  $\mathbf{B}$ ) flow or drift is much slower and is much less studied. We show in this paper that its consequences are far from negligible. Of special interest are effects that depend on  $\mathbf{B}_T$  direction, notably the power and particle flux distributions between the inner and outer divertor targets, and the spontaneous L-mode to H-mode transition power threshold. These cannot be explained by parallel physics. We concentrate on the  $\mathbf{E} \times \mathbf{B}_T$  plasma drift, because they are larger than the  $\nabla \mathbf{B}$  drifts near the edge [2–4]. Of course, all flows are strongly coupled in the edge, SOL and divertor, and full understanding of their consequences requires much additional work.

We highlight measurements from DIII-D tokamak plasmas that show unexpected local maxima of potential and electron pressure close to the  $X$ -point in L-mode, for both directions of the toroidal magnetic field.

\* Corresponding author. Tel.: +1-858 455 2841; fax: +1-858 455 4156.

E-mail address: schaffer@fusion.gat.com (M.J. Schaffer).

## 2. Experimental arrangement

The experiments were performed in the DIII-D tokamak [5] with an applied toroidal magnetic field  $B_T = 2.0\text{--}2.1$  T at radius  $R = 1.7$  m. Both the directions

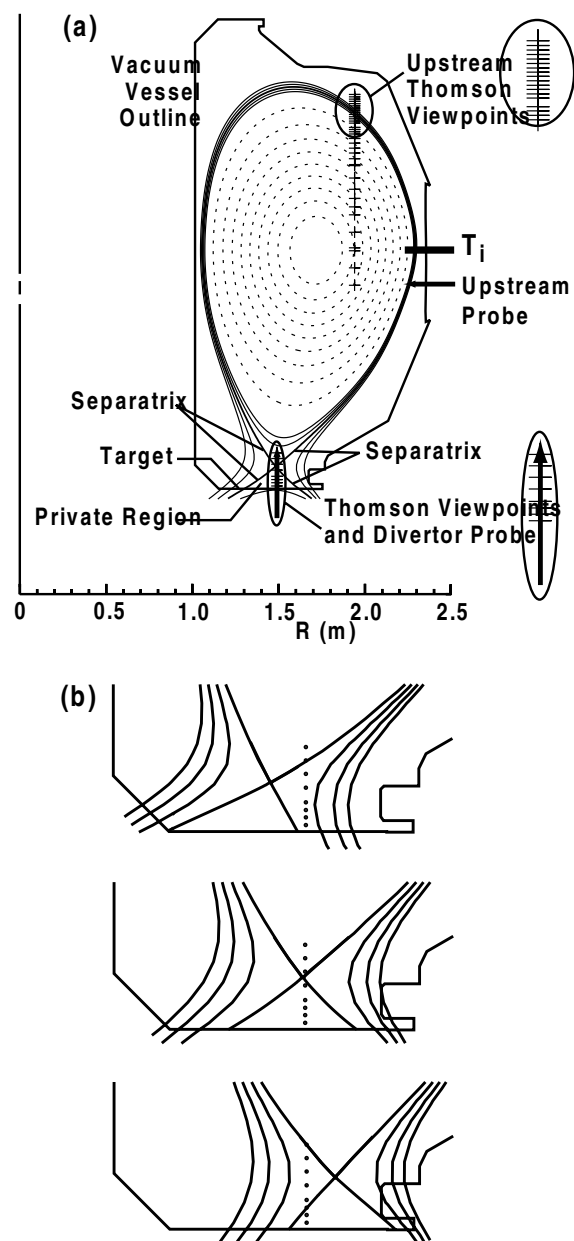


Fig. 1. (a) Single-null diverted plasma geometry shown inside the DIII-D vacuum vessel outline with the disposition of probe, Thomson scattering and ion temperature diagnostics. The 98% and 99% normalized flux surfaces are drawn inside the separatrix, and the 101% and 102% surfaces outside; (b) maximum range of divertor geometries used to measure outside and inside the X-point radius and through the X-point.

of  $B_T$  were employed, thereby changing the direction of  $B_T$ -dependent drifts. Neutral beam heating was used. The plasma was diverted by a single magnetic null to the lower target. Fig. 1 shows a typical geometry. In most cases, the X-point was located closer to the target than customary to provide diagnostic coverage above the X-point. The divertor plasma was attached to the target at the outer strike point and partially detached at the inner, which is typical in DIII-D.

Electric potential was measured by a pair of fast-stroking probe arrays, one moving vertically through the divertor region [6] and the other horizontally through the upstream SOL just below the torus equatorial plane [7]. Both probe stroke paths are indicated in Fig. 1(a). Langmuir probe tips on the arrays measured electron temperature  $T_e$  and the floating potential  $\Phi_f$ . The plasma potential  $\Phi$  was calculated from  $\Phi_f$  and  $T_e$  as usual. Two Thomson scattering systems provided the primary measurements of  $T_e$  and electron density  $n_e$ . The divertor Thomson scattering system [8] measured at eight vertically separated locations at the same radius as the divertor probe, as shown in Fig. 1. The ‘upstream’ Thomson scattering system [9] measured at many closely spaced points ( $\approx 13$  mm separation) vertically along the edge and SOL, as shown in Fig. 1(a). Plasma ion temperature  $T_i$  was measured near the equator by charge exchange recombination spectroscopy (CER) [10]. No suitable  $T_i$  diagnostic covers the X-point in DIII-D.

The X-point was magnetically stepped past the divertor diagnostics, between the extremes shown in Fig. 1(b), to obtain data in two dimensions. Magnetic surfaces were calculated by the equilibrium fitting code EFIT [11]. Surfaces are labeled by their normalized poloidal magnetic flux.  $\psi_n = 1$  is the separatrix, and  $\psi_n > 1$  is the SOL with  $\psi_n$  increasing outward from the separatrix.  $\psi_n < 1$  is either the closed confinement or open private region with  $\psi_n$  decreasing inward from the separatrix.

## 3. Results

We present potential and electron pressure results from low power L-mode plasmas, which display the most interesting X-point behavior. The plasmas had  $I_p = 1.0$  MA, line average electron density of  $2.5 \times 10^{19} \text{ m}^{-3}$ , and were heated by 0.3 MW of neutral beam and 0.6 MW of Ohmic power. Fig. 2 shows the upstream  $T_e$  and  $T_i$  profiles as functions of  $\psi_n$ . The plotted data are from a discharge with  $B_T$  directed into the page in Fig. 1 (‘reversed’  $B_T$ , ion  $\nabla B$  drift away from the X-point), for which we have the most complete data, but the profiles for ‘standard’  $B_T$  (ion  $\nabla B$  drift towards the X-point) are not markedly different. Note that  $T_i > T_e$  just inside and outside the equatorial separatrix, a well-known effect where the energy transport time out

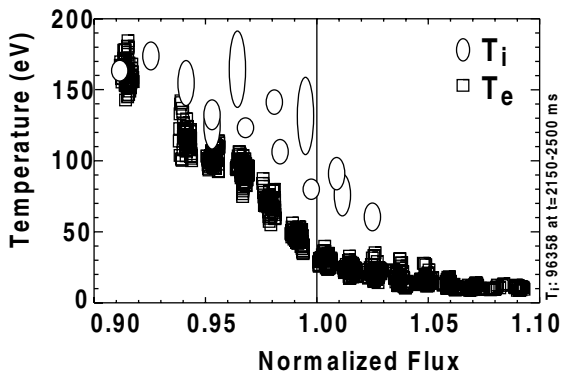


Fig. 2. Upstream ion and electron temperatures, measured by CER and Thomson scattering, respectively, as a function of  $\psi_n$ . Elliptical symbols indicate mean and standard deviation of three to five  $T_i$  measurements. The  $T_e$  time sequential data were smoothed somewhat prior to plotting for clarity.

of the edge layer becomes less than the electron–ion energy equilibration time. We will show that the high upstream  $T_i$  is partly responsible for the  $X$ -point po-

tential and  $p_e$  hills, whose discovery is one of the main results of this paper.

Fig. 3 shows  $n_e$ ,  $T_e$  and  $p_e = n_e T_e$  from Thomson scattering plotted as functions of  $\psi_n$  from the same reversed  $B_T$  L-mode shot as Fig. 2. The ‘ $X$ -region’ data cover three regions that meet at the  $X$ -point: inner SOL, outer SOL and closed or confinement surfaces. The data show that  $p_e$  near the  $X$ -point is more than two times greater than upstream on the same magnetic surfaces near the separatrix. Therefore, there is a previously unsuspected local  $p_e$  maximum or ‘hill’ near the  $X$ -point. The excess  $X$ -point  $p_e$  is greatest on closed surfaces and the outer divertor SOL and is least on inner SOL surfaces, at least within the field of view of the diagnostic. The  $p_e$  hill is observed in L-mode with both  $B_T$  directions and in the few Ohmically heated plasmas for which we have data. The  $X$ -point maxima extend inward for about 1% of poloidal flux from the separatrix. In contrast,  $p_e$  in H-mode remains constant on confinement surfaces (other shots, not shown). The  $p_e$  hill is not a consequence of either EFIT flux mapping or Thomson scattering errors. In these L-mode plasmas, the upstream edge gradients are small, and any remaining small EFIT er-

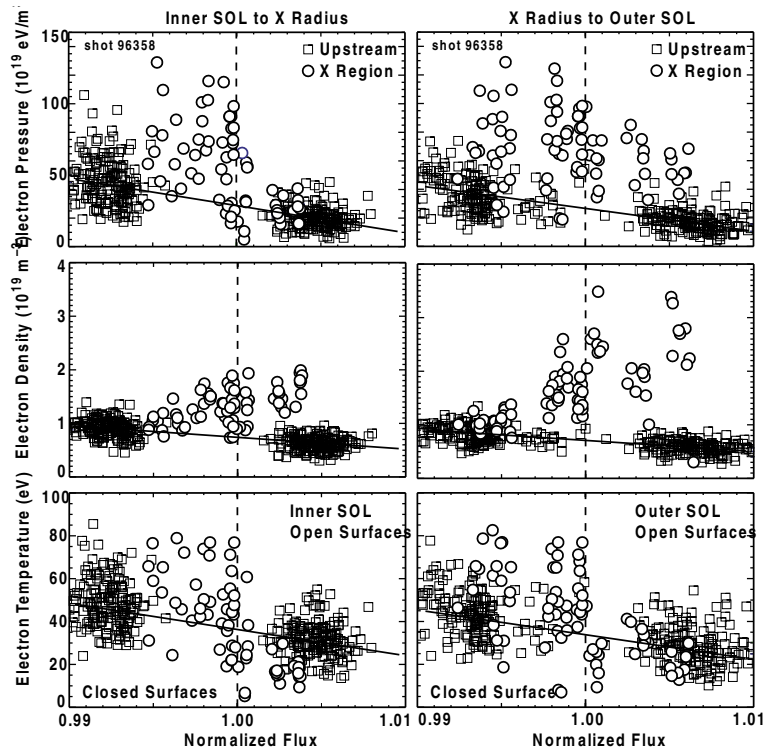


Fig. 3. Electron  $p_e$ ,  $n_e$  and  $T_e$ , measured by Thomson scattering, as a function of  $\psi_n$ . Data from upstream and the  $X$ -region are distinguished by their plot symbols.  $X$ -region data are from diagnostic view points ranging from just above to just below the  $X$ -point position; data from colder plasma near the target are excluded. Left plot combines data from part of the inner SOL and through the  $X$ -point. Right plot combines data from the outer SOL and through the  $X$ -point. Data through the  $X$ -point are common to both plots. The straight lines interpolate upstream data.

rors do not significantly change the upstream  $p_e(\psi_n)$ , etc. Near the  $X$ -point, the expanded flux means that mapping divertor diagnostic coordinates to the  $\psi_n$  coordinate is very insensitive to EFIT errors. The Thomson data validity was verified, and the Thomson scattering and Langmuir probe measurements agree. The fact that the divertor and upstream density profiles in Fig. 3 merge together at about 1% of poloidal flux away from the separatrix means that there is no systematic discrepancy between the divertor and upstream Thomson density measurements. Channel-to-channel divertor Thomson scattering errors were additionally ruled out by comparison of data as the divertor geometry varied, bringing the same region of plasma successively into the view of different channels. The expected jump of  $T_e$  across the  $X$ -point separatrix is clearly seen in the bottom panels of Fig. 3.

The  $p_e$  hill is associated mainly with a corresponding greater  $n_e$  near the  $X$ -point relative to upstream. However, as seen in the figure,  $T_e$  inside the separatrix is also locally somewhat higher near the  $X$ -point ( $\sim 55$  eV) than upstream ( $\sim 35$  eV) and contributes to the  $p_e$  hill. The higher  $X$ -point  $T_e$  is less prominent or absent with standard  $B_T$ . We do not have a satisfactory explanation for the locally higher  $T_e$ . We checked the diagnostics extensively, as discussed in the preceding paragraph.

Fig. 4 shows plasma potential plotted as a function of  $\psi_n$  in all four  $X$ -regions of the same reversed  $B_T$ , L-mode shot as Fig. 2. Despite large fluctuations at  $\lesssim 100$  Hz, which are characteristic of both  $\Phi$  and  $T_e$  near the L-mode separatrix [12], the near- $X$ -potentials are positive ( $\sim 100$  V) and much larger than the potentials upstream ( $\sim 20$  V) on the same magnetic surface. In shots with standard  $B_T$ , the  $X$ -region potentials were similarly distributed but were  $\sim 50$  V more positive, while the upstream potentials were only  $\sim 25$  V more positive. A similar  $X$ -point  $\Phi$  was also reported in the outer SOL and just inside the separatrix of an earlier DIII-D L-mode discharge [12], but the rest of the  $X$ -point region was not explored. We conclude that a large positive electric potential hill exists near the  $X$ -point, extending into the SOL, confinement and private flux surfaces in L-mode plasmas. The large potential difference between the  $X$ - and upstream locations on closed surfaces is remarkable, because neoclassical plasma theory predicts only a weak poloidal potential variation,  $e\Delta\Phi \ll kT_e$ . In the SOL, the non-monotonic poloidal potential variation, from target ( $\Phi = 0$ ) to potential hill in the  $X$ -region to a modest value upstream, is also noteworthy, because it is commonly thought, based on simplified application of the parallel plasma Ohm's law, that  $\Phi$  should increase monotonically with  $T_e$ . ( $T_e \sim 5$  eV at the target in these low power plasmas.) Clearly it does not.

Fig. 5 shows divertor plasma potential from a standard  $B_T$ , ELMy H-mode plasma. It had  $I_p = 1.4$  MA, line average electron density of  $6 \times 10^{19} \text{ m}^{-3}$ , and 3.5

MW of neutral beam heating. The upstream probes have not yet reliably measured potentials inside the upstream separatrix in H-mode, because the high power density overheats the probe tip.

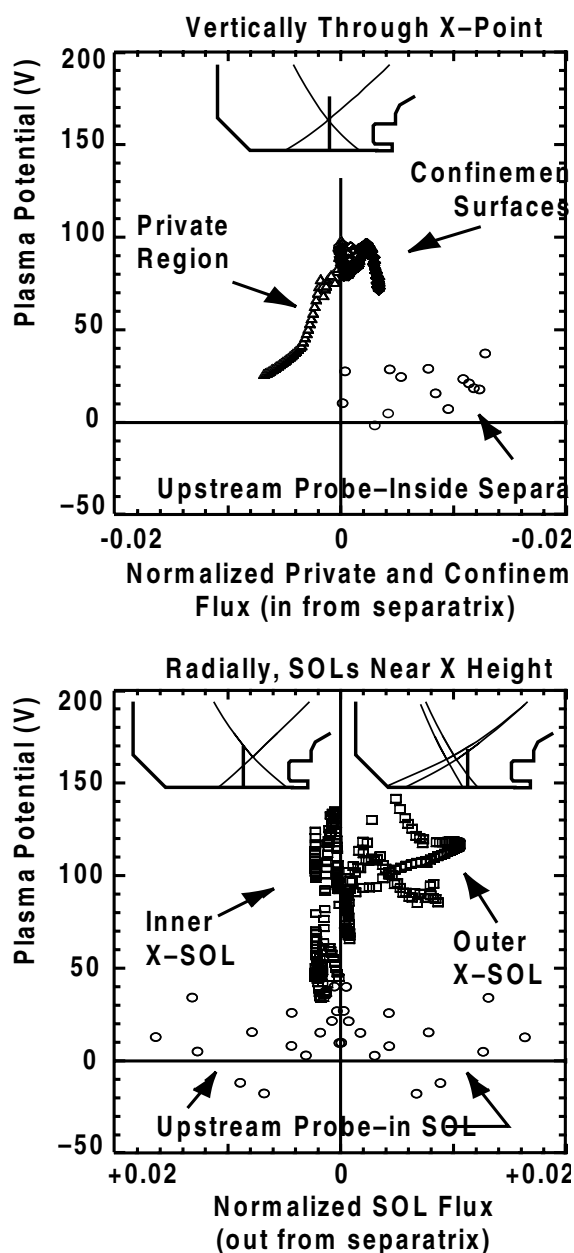


Fig. 4. Potential  $\Phi$  plotted as a function of  $\psi_n$ . Target is at  $\Phi = 0$ . Divertor data extend from somewhat below the  $X$ -point to somewhat above it. Upper plot shows data from a probe stroke through the private region, the  $X$ -point and into the confinement surfaces. Lower plot combines one inner SOL and two outer SOL strokes into a limited radial scan at near  $X$ -point height. Upstream data combine two strokes.

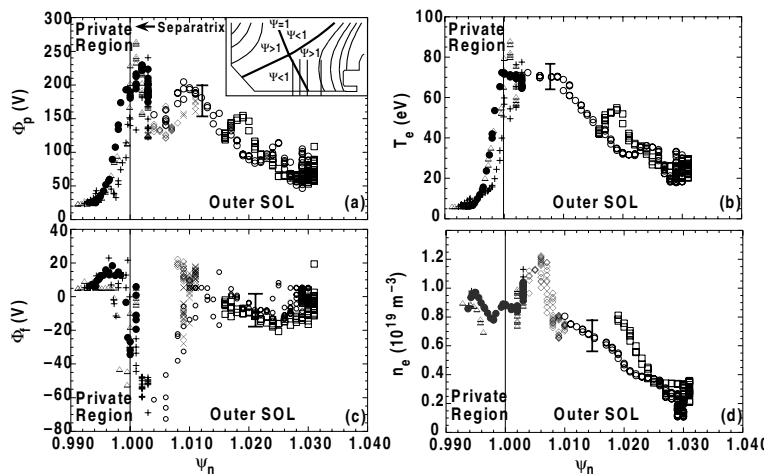


Fig. 5. Measured outer divertor profiles as a function of  $\psi_n$ , from an ELMy H-mode plasma: (a) plasma potential  $\Phi$ ; (b)  $T_e$ ; (c) floating potential  $\Phi_f$ ; (d)  $n_e$ . Inset shows equivalent divertor probe trajectories schematically. Different symbols indicate different probe strokes.

#### 4. X-point circulation

The electric field emanating from the potential hill drives a poloidal-like circulation on equipotentials around the X-point, sketched qualitatively in Fig. 6, at the electric drift velocity,  $\mathbf{v}_E = \mathbf{E} \times \mathbf{B} / B^2 \approx -\nabla\Phi \times \mathbf{B}_T / B_T^2$ , where we use  $\mathbf{B} \approx \mathbf{B}_T$  in a tokamak. The poloidal gradient causes plasma drift normal to surfaces, both closed and open. The radial potential gradient causes drift in the poloidal direction. The divertor drift,

especially the drift across the private region, has been discussed theoretically [3,4] and observed experimentally [13]. The private drift was shown to be the main factor contributing to the long-observed sensitivity of the inner–outer divertor target plasma differences to the  $B_T$  direction. The newly observed potential hill on closed surfaces near the X-point, reported above, extends the circulation into the confinement volume.

The number of particles per second  $\dot{N}$  convected outward by  $\mathbf{v}_E$  through a ribbon surface defined by the rotation of a curve C about the major axis (see Fig. 7) and bounded by potentials  $\Phi_1$  and  $\Phi_2$  is [13]

$$\begin{aligned} \dot{N} &= \int_1^2 2\pi R n v_E (\hat{\mathbf{e}}_\phi \times ds) \approx 2\pi \int_1^2 \frac{Rn}{B_T} (\nabla\Phi) \cdot ds \\ &= 2\pi \int_{\Phi_1}^{\Phi_2} \frac{Rn}{B_T} d\Phi. \end{aligned} \tag{1}$$

If  $B_T$ ,  $R$  and  $n$  are nearly constant across the potential gradient region, this simplifies to

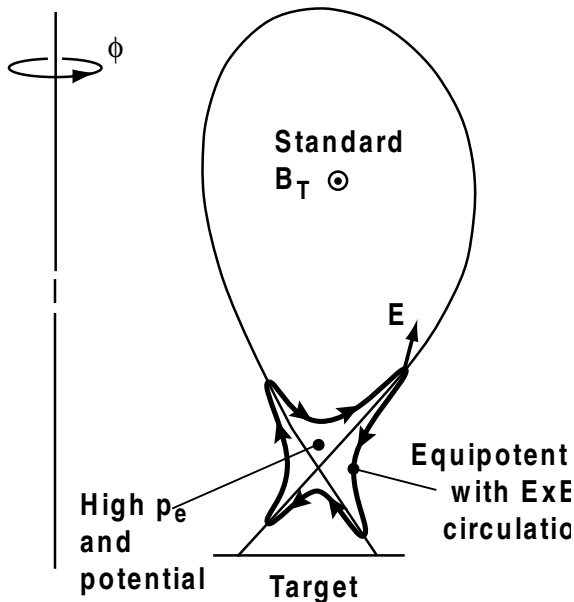


Fig. 6. Illustration of  $\mathbf{E} \times \mathbf{B}$  circulation around the X-point driven by the positive potential hill.

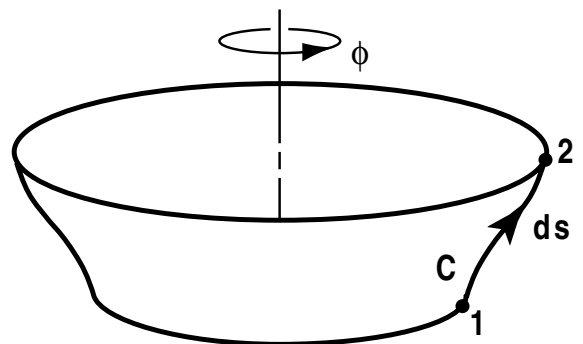


Fig. 7. Integration path used to calculate  $\mathbf{E} \times \mathbf{B}$  convection across an axisymmetric ribbon surface.

$$\dot{N} \approx (2\pi/R_0 B_0) \langle nR^2 \rangle (\Phi_1 - \Phi_2) \quad (2)$$

and  $\dot{N}$  depends just on the potential difference across the plasma flow layer, no matter how oriented. Here  $\langle \dots \rangle$  means average along C, and  $B_0$  is the toroidal magnetic field at some major radius  $R_0$ .

Consider first  $\dot{N}$  on the private region side of the potential gradient from the ELMy H-mode data of Fig. 5. Using  $R_0 B_0 = (1.7 \text{ m})(2.1 \text{ T}) = 3.57 \text{ T m}$ ,  $\langle nR^2 \rangle \approx (1 \times 10^{19} \text{ m}^{-3})(1.6 \text{ m})^2$ , and  $\Delta\Phi \approx 200 \text{ V}$  yields  $\dot{N} \approx 1 \times 10^{22} \text{ s}^{-1}$  which is convected from the outer to the inner target. The measured ion flow to the inner and outer targets is  $\approx 3 \times 10^{22} \text{ s}^{-1}$ , so the private  $\mathbf{E} \times \mathbf{B}_T$  flow is *prima facie* important. The divertor leg potential remains positive with reversed  $\mathbf{B}_T$  direction, so the  $\mathbf{E} \times \mathbf{B}_T$  direction reverses with  $\mathbf{B}_T$ . UEDGE numerical simulation with drifts of a generic DIII-D H-mode shot predicted  $\dot{N} \approx 0.7 \times 10^{22} \text{ s}^{-1}$  [3] about the same as measured. The simulations also demonstrated that the private region  $\mathbf{E} \times \mathbf{B}_T$  flow is the principal factor governing the  $\mathbf{B}_T$  direction sensitivity of the power and particle flux distributions between the inner and outer divertor targets [3]. Other DIII-D divertor  $\mathbf{E} \times \mathbf{B}_T$  flow results are given in [13,14].

Convection of the confined plasma across the separatrix, between the  $X$ -point and upstream, can be calculated in the same way from Eq. (2) and data in Figs. 3 and 4. Taking  $n \approx 1.1 \times 10^{19} \text{ m}^{-3}$  as the mean density between the  $X$ -point and the equator, and  $\Delta\Phi = 65 \text{ V}$  yields  $\dot{N} \approx 3 \times 10^{21} \text{ s}^{-1}$ . This is more than half of the estimated cross-separatrix transport of  $\approx 5 \times 10^{21} \text{ s}^{-1}$  for this shot. The convected power  $P$  due to this circulation is calculated by replacing  $n$  by  $5p/2$  in Eq. (2). Taking  $p \approx 195 \text{ Pa}$  near the  $X$ -point yields  $P \approx 0.14 \text{ MW}$ , which is about 20% of the 0.7 MW total power crossing the separatrix. The toroidal angular momentum convected per second by the circulation across the separatrix is calculated by replacing  $n$  by  $m_i n \Omega R^2$  in Eq. (2), where  $\Omega$  is the toroidal rotation angular frequency. From CER measurements,  $\Omega \approx 3500 \text{ s}^{-1}$ , so the convected angular momentum rate is about 0.14 N m, compared with 0.165 N m injected by the neutral beam. We do not have adequate data to do a similar calculation for poloidal angular momentum.

The  $X$ -point  $\mathbf{E} \times \mathbf{B}_T$  volume exchange time  $\tau_X = |AB/\Delta\Phi|$ , where  $A$  is the poloidal area of interest, characterizes all  $\mathbf{E} \times \mathbf{B}_T$  convection. For the area bounded by the separatrix, the  $\psi_n = 0.99$  surface, and extending part way upstream (this last boundary is not covered by any diagnostic and is not known),  $A \approx 0.01 \text{ m}^2$ . Then  $\tau_X \sim 0.4 \text{ ms}$ . It is much shorter than the ion–neutral charge exchange time,  $(n_0 \langle \sigma_{\text{ex}} v_i \rangle)^{-1}$ , which is  $\gtrsim 3 \text{ ms}$  for  $n_0 \lesssim 1 \times 10^{16} \text{ m}^{-3}$ , as measured in another shot at the same density and standard  $B_T$  direction [15]. Therefore, charge exchange, which has been advanced as significant mechanism to remove plasma

angular momentum [16,17], removes about an order of magnitude less angular momentum than the  $X$ -point  $\mathbf{E} \times \mathbf{B}$  circulation.

### 5. X-point potential generation

We explain the L-mode  $X$ -point potential and  $p_e$  hills as a consequence of the variation of the ion pressure  $p_i$  along a magnetic flux tube wherein the total pressure  $p = p_e + p_i$  remains constant. First, from Figs. 3 and 4, just inside the upstream separatrix, we have  $n_e \approx n_i \approx 0.75 \times 10^{19} \text{ m}^{-3}$ ,  $T_e \approx 35 \text{ eV}$  and  $p_e \approx 26 \times 10^{19} \text{ eV m}^{-3}$ ;  $T_i \approx 125 \text{ eV}$  and  $p_i \approx 94 \times 10^{19} \text{ eV m}^{-3}$ . The total upstream pressure is  $120 \times 10^{19} \text{ eV m}^{-3}$ . Similarly, near the  $X$ -point separatrix, we have  $n_e \approx n_i \approx 1.5 \times 10^{19} \text{ m}^{-3}$ ,  $T_e \approx 55 \text{ eV}$  and  $p_e \approx 82 \times 10^{19} \text{ eV m}^{-3}$ .  $T_i$  is not measured, but invoking uniformity of the total pressure, the  $X$ -point  $p_i \approx 38 \times 10^{19} \text{ eV m}^{-3}$ , and then  $X$ -point  $T_i \approx 25 \text{ eV}$ .  $X$ -point  $p_i$  and  $T_i$  are much lower than upstream. The  $p_e$  hill is sustained along a magnetic flux tube by the parallel electric field. According to the parallel component of the electron momentum equation [18]

$$\begin{aligned} e\nabla_{\parallel}\Phi &= -eE_{\parallel} = \nabla_{\parallel}p_e/n_e + 0.71\nabla_{\parallel}kT_e \\ &= \nabla_{\parallel}(p - p_i)/n_e + 0.71\nabla_{\parallel}kT_e, \end{aligned} \quad (3)$$

the potential is high where  $p_i$  is low and  $n_e$  is large, as at the  $X$ -point. Estimating  $\Delta\Phi$  from Eq. (3) and the measured  $p_e$ ,  $n_e$ , and  $T_e$  yields a  $X$ -point potential about 65 V higher than the upstream, which is consistent with the potential data in Fig. 4. The  $X$ -point  $n_e$  hill arises from redistribution of the plasma particles to satisfy the parallel equilibrium and does not depend on, e.g., a  $X$ -point gas source.

We do not know if the potential and  $p_e$  hills and the low  $X$ -point  $T_i$  are universal features of diverted L-mode plasmas, or if they are a special case. The mechanism identified here requires that  $T_i$  be clamped to a lower value at the  $X$ -point than upstream. Classical ion parallel thermal conduction power from equator to  $X$ -point in the heterogeneous layer between the separatrix and  $\psi_n = 0.995$  is small in the plasmas reported here, calculated to be  $\approx 0.08 \text{ MW}$ . Ion–electron energy exchange at  $\sim 0.01 \text{ MW}$  is negligible, as is ion cooling to neutrals. However, convection of cool ions in across the separatrix and hot ions out by the  $X$ -point circulation can remove up to  $\sim 0.1 \text{ MW}$  by the calculation in Section 4, if ions are much cooler in the SOL near the  $X$ -point than on the nearby closed surfaces. This is not implausible, because, as seen in Fig. 6, the circulation draws plasma upstream from the nearby target. Therefore, the  $X$ -point heterogeneity might be a self-consistent, self-sustaining state. Numerical modeling of a two fluid plasma with drifts and realistic  $X$ -point geometry, as in [3,4], is

needed to verify whether this model is quantitatively adequate.

## 6. Additional discussion

The observed absence of an  $X$ -point  $p_e$  hill in H-mode plasmas implies the absence of a potential hill and  $X$ -point circulation in H-mode. Since H-mode is characterized by a narrow edge transport barrier, we *speculate* that suppression of the  $X$ -point circulation might be important for the spontaneous L–H transition in poloidally diverted plasmas. Transition would then require homogenization of  $T_i$  on each magnetic surface, e.g., by exceeding a threshold heating power. Poloidal homogenization was a feature of electrode-driven L–H transitions in the CCT limiter tokamak [19]. The  $B_T$  direction dependence would arise from ion energy convected into or out of the heterogeneous  $X$ -point region by, e.g., the vertical ion  $B$  and curvature drift velocity, much as proposed by Hinton [20]. Further work is needed to develop and test this idea.

## 7. Conclusion

An electric potential hill and an associated electron pressure hill were discovered at the divertor  $X$ -point in L-mode plasmas. The potential hill drives a strong  $\mathbf{E} \times \mathbf{B}_T$  circulation of ions across the separatrix and extends the previously reported divertor  $\mathbf{E} \times \mathbf{B}_T$  circulation to closed magnetic surfaces. The potential is consistent with classical parallel plasma physics, when the  $X$ -point  $T_i$  is clamped lower than the upstream  $T_i$ . The low local  $T_i$  state might be self-sustaining due to the same  $\mathbf{E} \times \mathbf{B}_T$  circulation. We speculate that if the circulation is incompatible with H-mode, the spontaneous L–H transition might not start until  $T_i$  equalized on the near-separatrix magnetic surfaces.

## Acknowledgements

The authors acknowledge helpful discussion and contributions from D.R. Baker, B.D. Bray, K.H. Burrell, C.J. Lasnier, A.W. Leonard, G.D. Porter, and T.D. Rognlien. This work was supported by the US Department of Energy under Contracts DE-AC03-99ER54463, DE-AC04-94AL85000, and Grant No. DE-FG03-95ER54294.

## References

- [1] F.L. Hinton, Y-B. Kim, Nucl. Fus. 34 (1994) 899.
- [2] A.V. Chankin et al., Plasma Phys. Control. Fus. 36 (1994) 1853.
- [3] T.D. Rognlien et al., J. Nucl. Mater 266–269 (1999) 654.
- [4] T.D. Rognlien et al., Phys. Plasmas 6 (1999) 1851.
- [5] J.C. Luxon, L.G. Davis, Fus. Technol. 8 (1985) 441.
- [6] J.G. Watkins et al., Rev. Sci. Instrum. 68 (1997) 373.
- [7] J.G. Watkins et al., Rev. Sci. Instrum. 63 (1992) 4728.
- [8] T.N. Carlstrom et al., Rev. Sci. Instrum. 68 (1997) 1195.
- [9] T.N. Carlstrom et al., Rev. Sci. Instrum. 63 (1992) 4901.
- [10] P. Gohil et al., in: Proceedings of the 14th Symposium on Fusion Engineering (San Diego, 1991), vol. 2, IEEE, New York, 1992, p. 1199.
- [11] L.L. Lao et al., Nucl. Fus. 25 (1985) 1681.
- [12] R.A. Moyer et al., J. Nucl. Mater 266–269 (1999) 1145.
- [13] J.A. Boedo, M.J. Schaffer et al., Phys. Plasmas 7 (2000) 1075.
- [14] J.A. Boedo et al., in: Proceedings of the 26th EPS Conference on Control Fusion and Plasma Physics (Maastricht, 1999), ECA 23J, 1999, p. 1185.
- [15] R.J. Colchin et al., Nucl. Fus. 40 (2000) 175.
- [16] M.A. Mahdavi et al., J. Nucl. Mater. 176&177 (1990) 32.
- [17] B.A. Carreras et al., Phys. Plasmas 5 (1998) 2623.
- [18] S.I. Braginskii, in: M.A. Leontovich (Ed.), Reviews of Plasma Physics, vol. 1, Consultants Bureau, New York, 1965, p. 205.
- [19] G.R. Tynan et al., Plasma Phys. Control. Fus. 38 (1996) 1301.
- [20] F.L. Hinton, Nucl. Fus. 25 (1985) 1457.